Journal of Physiology (1992), **456**, *pp.* 325–349
With 13 figures
Printed in Great Britain

AN ANALYSIS OF THE LONG-LASTING AFTER-HYPERPOLARIZATION OF GUINEA-PIG VAGAL MOTONEURONES

BY SONIA D. HOCHERMAN, R. WERMAN AND Y. YAROM

From the Department of Neurobiology, Life Sciences Institute, Hebrew University, Jerusalem 91904, Israel

(*Received 11 October 1991*)

SUMMARY

1. The long-lasting after-hyperpolarization which characterizes the neurones of the dorsal motor nucleus of the vagus in the guinea-pig was studied *in vitro*.

2. Following a train of action potentials, vagal motoneurones develop a long-lasting after-hyperpolarization. Two different shapes of long-lasting after-hyperpolarization were encountered: an after-hyperpolarization which slowly (0·6–1·2 s) and monotonically developed to peak value; and a second type of long-lasting after-hyperpolarization where the onset of the slow component appears to be masked by an early, relatively fast component. Both shapes of long-lasting after-hyperpolarization depend on Ca^{2+} influx and increase as a function of the number of action potentials in the train.

3. A novel procedure was used to analyse the ionic processes which underlie the long-lasting after-hyperpolarization. The neuronal responses to a series of long (7 s) hyperpolarizing current pulses during the long-lasting after-hyperpolarization were recorded and the voltage–current curves at 600 different time points along the long-lasting after-hyperpolarization were plotted. The conductance and the reversal potential at each time point were calculated from the slope and the intersection of these curves, respectively.

4. Using this procedure it was found that the long-lasting after-hyperpolarization consists of two conductances that differ in kinetic properties and reversal potential: an early conductance which peaks shortly after the end of the train and decays in a few tenths of seconds (EAHP), and a late conductance which develops slowly (time to peak about 1 s) and decays in 3–8 s (LAHP). The reversal potential for the early conductance is 10 mV more positive than the reversal potential for the late conductance (−84 mV); the latter reversal potential is in agreement with the K^+ equilibrium potential. The different shapes of long-lasting after-hyperpolarization can be explained by different ratios of these two conductances.

5. Noradrenaline (10 μM) selectively blocks the late conductance, without an observable effect on the Ca^{2+} action potential.

6. The behaviour of the noradrenaline-sensitive late conductance was analysed. The amplitude of the conductance change increased sigmoidally as a function of the number of spikes in the train. A log–log plot suggests that at least two Ca^{2+} ions participate in the opening of a K^+ channel.

MS 9808

7. A model that accounts for the slow kinetics of the late conductance was constructed. The model assumes that two Ca^{2+} ions are needed to open a potassium channel and that the intracellular Ca^{2+} concentration reaches its maximum value at the end of the train of action potentials. It was found that under these assumptions, the onset of the LAHP is governed by the channel's rate constants and the initial increase in Ca^{2+} concentration, whereas its duration is determined by the rate of removal of Ca^{2+} from the cell. The processes which might underlie the slow rate constants are discussed.

INTRODUCTION

During the last decade, with the development of *in vitro* systems to study the electrical behaviour of neurones from the mammalian central nervous system, it has been established that Ca^{2+}-dependent K^+ conductances, first described by Meech & Standen (1975) in invertebrates, play a crucial role in moulding the firing patterns of neurones (see Marty, 1989). It is commonly agreed that the long-lasting hyperpolarizations seen in most CNS neurones reflect the activation of K^+ conductances which are triggered by an increase in intraneuronal Ca^{2+} concentration following Ca^{2+} influx during spike activity. The different types of Ca^{2+}-dependent K^+ conductances that have been described over the years differ in their kinetic properties, single-channel conductance and voltage sensitivity. Since these conductances determine the behaviour of the membrane potential during the interspike interval, they give rise to a variety of firing patterns. The long-lasting time course of these conductances has been often postulated to reflect the time course of the changes in intracellular Ca^{2+} concentration (Herman & Gorman, 1981; Kuba, Morita & Nohmi, 1983). In some vertebrate preparations, however, the Ca^{2+}-dependent after-hyperpolarization reaches its peak a long time after the end of the train of action potentials (Gustafsson & Wigstrom, 1981; Morita, North & Tomikasa, 1982; Lancaster & Adams, 1986; Yoshimura, Polosa & Nishi, 1986, 1987; Constanti & Sim, 1987; Lancaster & Nicoll, 1987). Since it is assumed that the increase in Ca^{2+} concentration reaches its maximum value during or soon after the burst of activity, it is difficult to explain the slower onset of some of the Ca^{2+}-dependent K^+ conductances.

In this work, the properties of a slowly developing, long-lasting Ca^{2+}-dependent K^+ conductance have been studied in neurones from the dorsal motor nucleus of the vagus. To this end, a method for continuously monitoring the changes in conductance and in reversal potential during the after-potential was developed and a pharmacological procedure to dissect this conductance was found. Using these two tools it was possible to accurately define the time course of the conductance change, to determine its ionic specificity and to integrate the kinetic studies into a comprehensive and yet simple model which simulates the slow time course and predicts its behaviour. Some of these results were previously presented as an abstract (Hocherman, Werman & Yarom, 1988).

METHODS

The submerged slice technique, previously described (Llinas & Sugimori, 1980; Yarom, Sugimori & Llinas, 1985*b*) was used throughout this work. Briefly, guinea-pigs weighing 200–500 g were anaesthesized with sodium pentobarbitone, decapitated, and the brainstem was exposed, removed

and transferred to a vial of cold oxygenated Krebs solution, composed of (mM): 124 NaCl, 5 KCl, 1·2 $MgSO_4$, 1·2 KH_2PO_4, 26 $NaHCO_3$, 2·3 $CaCl_2$, 10 glucose. The brainstem was then sliced with an Oxford vibratome sectioning system into sagittal or coronal sections of 400 μm. The slices were stored at room temperature in vials filled with normal Krebs solution bubbled continuously with 95% O_2 and 5% CO_2.

Intracellular recordings were made from a single slice transferred into a recording chamber where it was continuously superfused with preheated, oxygenated Krebs solution, usually at 33 °C. The glass microelectrodes were filled with a saturated solution of potassium acetate and an Axoclamp-2A amplifier was used for intracellular recordings. The recordings were either stored on tape or directly averaged on a Nicolet Digital Oscilloscope 4094 and stored on diskettes using a Nicolet F-43 Disk Recorder. For analysis and illustrations the data were transferred from the Nicolet to an IBM-PC computer and processed with the help of Lotus (TM) or Grapher (TM) softwares.

RESULTS

Characterization of the long-lasting after-hyperpolarization

In the vagal motoneurone, a brief train of action potentials elicits a long-lasting after-hyperpolarization. The shape, amplitude and duration of this long-lasting after-hyperpolarization can vary significantly in different cells. Figure 1 shows two examples of long-lasting after-hyperpolarizations (*A* and *C*) generated in two different neurones by trains of four action potentials, each elicited by a brief current pulse. The long-lasting after-hyperpolarization frequently develops slowly (Fig. 1*A*), reaching a peak (*) roughly 1 s after the last action potential and lasting several seconds. We refer to this slowly developing and long-lasting after-hyperpolarization as the late after-hyperpolarization (LAHP). Examination of the period during and shortly after the train of action potentials (Fig. 1*B*) shows that each action potential is followed by an after-hyperpolarization, which is probably the expression of the voltage-dependent Hodgkin–Huxley K^+ conductance ($g_{K,H-H}$). Following the after-hyperpolarization of the last action potential (○), the membrane potential starts to repolarize with a time constant close to that of the passive membrane of the neurone. After 20 ms (first arrowhead), the rate of repolarization slows down and the membrane potential stays almost constant for a relatively long time (about 200 ms, between the arrowheads in 1*B*). At the time indicated by the second arrowhead in Fig. 1*B*, the membrane begins to hyperpolarize once again and the LAHP slowly develops (arrow, Fig. 1*A*). The long period (200 ms) of almost constant hyperpolarization raises the possibility that at this time another process may participate in the generation of the long-lasting after-hyperpolarization.

An example of a second type of long-lasting after-hyperpolarization is shown in Fig. 1*C* and *D*; the shape of the long-lasting after-hyperpolarization is consistent with the possibility that two hyperpolarizing components participate in its generation. In Fig. 1*C*, the amplitude of the LAHP (*) is rather small, and its onset is masked by an early after-hyperpolarization (arrow), which lasts for about 300 ms. This early after-hyperpolarization (EAHP) can be seen better in Fig. 1*D*; it is different from the fast after-hyperpolarization that follows each action potential. The latter, as in the previous example (Fig. 1*B*), decays with a time constant of a few milliseconds and probably results from activation of $g_{K,H-H}$. The EAHP is usually prominent in cells in which the amplitude of the LAHP is small.

The amplitude of the long-lasting after-hyperpolarization is related to the number of action potentials used to elicit it; this dependence is shown in Fig. 2 for the two

cells already illustrated. Figure 2*A* shows four superimposed records of the long-lasting after-hyperpolarization following one, two, three and five action potentials. It can be clearly seen that the amplitude of the LAHP increases as a function of the number of action potentials. The dependence of the LAHP amplitude on the number

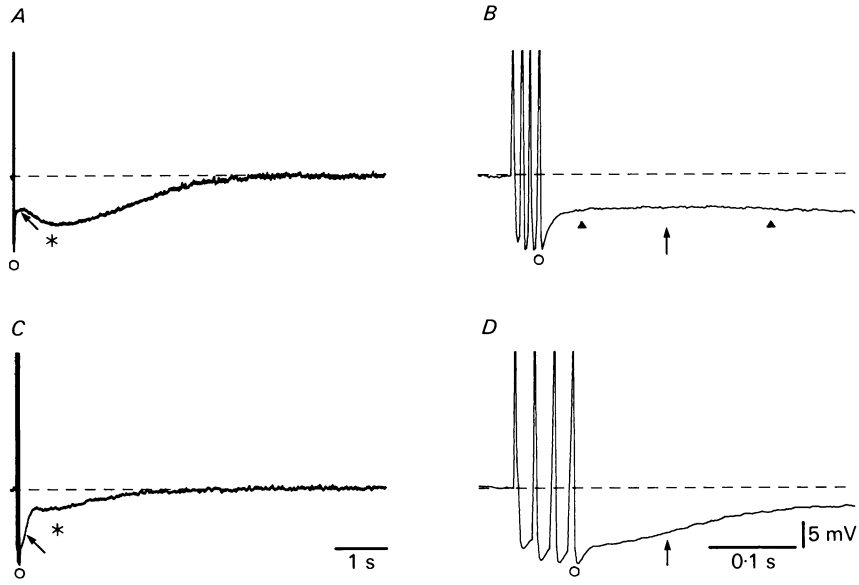

Fig. 1. Two types of long-lasting after-hyperpolarization recorded intracellularly from two vagal motoneurones. The long-lasting after-hyperpolarizations were evoked by trains of four action potentials and displayed a slow and fast recording speed. The action potentials were elicited by short depolarizing current pulses (5 ms, 1 nA). *A*, an initial delay (arrow in *A*) precedes the long-lasting after-hyperpolarization which develops slowly, reaching a peak after 800 ms (*). At a faster recording rate (*B*), the after-hyperpolarization (AHP) that follows each action potential can be discerned. After an initial decay of the fourth AHP (○), the membrane potential is maintained for about 200 ms (between arrowheads in *B*). In another cell (*C*), the long-lasting after-hyperpolarization (*) is less prominent, and its onset is masked by the presence of an early after-hyperpolarization (arrow). A faster recording rate (*D*), revealed that the early after-hyperpolarization lasts for about 300 ms, and that it appears at the same time as the maintained potential at *B*.

of action potentials is plotted in Fig. 2*C*. While the amplitude of the responses to one, two and three action potentials increases linearly, the amplitude reaches saturation after about five action potentials.

The long-lasting after-hyperpolarizations shown in Fig. 2*B* were obtained from a cell where both the EAHP and the LAHP are clearly recognizable. Both components appear to be affected by the number of action potentials. Although the amplitude of the EAHP only changes slightly, its duration does increase with the number of eliciting action potentials. The amplitude of the LAHP, however, behaves qualitatively similarly to the example shown in Fig. 2*A*. It should be noted that unlike the example shown in Fig. 2*C*, the amplitude appears to be a sigmoidal function of the number of action potentials (Fig. 2*D*).

The long-lasting after-hyperpolarization is triggered by the entry of external Ca^{2+} ions into the cell during the action potentials (see Yarom *et al.* 1985*b*). Figure 3 shows that both types of long-lasting after-hyperpolarization are virtually abolished when we substitute all the Ca^{2+} by Mg^{2+} ions (10 mM). The two superimposed traces (upper

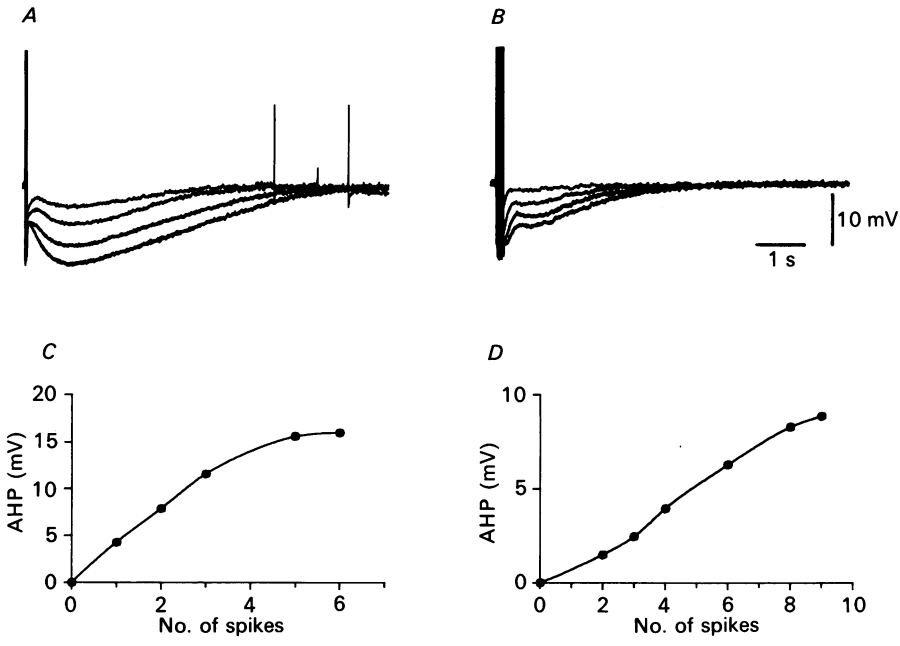

Fig. 2. The long-lasting after-hyperpolarization increases as a function of the number of action potentials. *A*, long-lasting after-hyperpolarizations elicited by trains of one, two, three and five action potentials. Each record represents the average of five traces. *C*, the maximal amplitude of the long-lasting after-hyperpolarization as a function of the number of action potentials in the train. Note that the initial linearity turns into a saturated process at trains longer than five action potentials. *B* and *D*, measuring the late component for another cell showing a prominent early component. The long-lasting hyperpolarizations were elicited by trains of two, four, six and eight action potentials. Note that both components of the long-lasting hyperpolarization seem to increase as a function of the number of action potentials in the train. Note also the sigmoidal relationship between the late component amplitude and the number of action potentials (*D*).

panels) demonstrate the responses of two cells to a short burst of action potentials before and after the replacement of Ca^{2+} ions. The lower panels give the difference between these two traces (subtraction of the traces). In the response of the cell shown in Fig. 3*A* the LAHP (the late component) was a prominent fraction of the long-lasting after-hyperpolarization and therefore the lower trace (the difference) roughly illustrates the time course of the LAHP. In the example shown in Fig. 3*B*, where both components (the LAHP and the EAHP) could be readily recognized, the lower trace demonstrates that both components are strongly reduced by blocking Ca^{2+} entry. It should be noted that in the presence of Mg^{2+} ions the after-potentials were not completely abolished. In Fig. 3*A* a slow component is visible following the rapid

phase of decay and in Fig. 3*B* the 70 ms time constant of decay cannot be attributed to the membrane time constant. It is likely, therefore, that the long-lasting after-hyperpolarization includes a non-Ca^{2+}-dependent component or that under our experimental conditions the Ca^{2+} influx during the action potential has not been completely blocked.

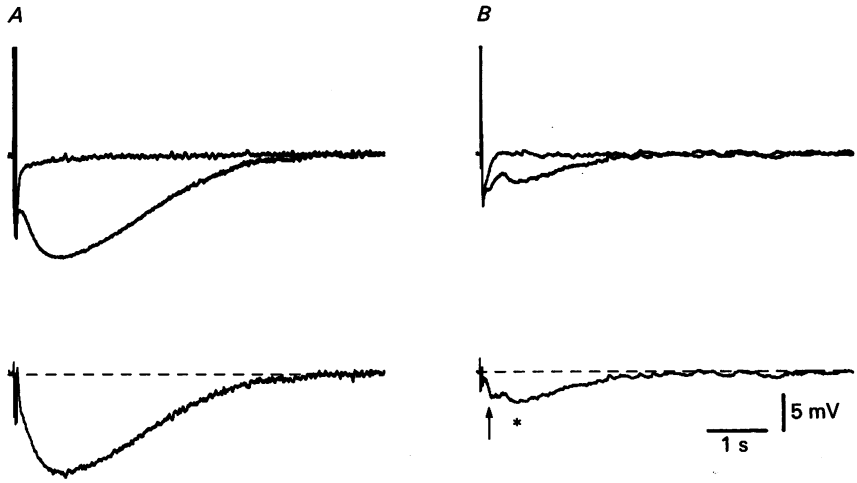

Fig. 3. The calcium dependence of the long-lasting after-hyperpolarization. *A*, upper panel: superimposed records of the long-lasting after-hyperpolarizations (elicited by trains of four action potentials) with a prominent late component before and after substituting the 2·5 mM-Ca^{2+} ions by 10 mM-Mg^{2+} ions. Note that in the presence of Mg^{2+} ions the membrane potential repolarizes with a time constant of 14 ms. Lower panel: subtraction of the two upper traces shows the time course of the Ca^{2+}-dependent voltage changes. Notice the slow time to peak, characteristic of the late component of the long-lasting after-hyperpolarization. *B*, upper panel: in another cell, a train of three action potentials in the presence of Ca^{2+} elicits a long-lasting after-hyperpolarization with a clear early component. After substitution of Ca^{2+} by Mg^{2+} ions, the membrane potential repolarizes with a time constant of 70 ms. Subtraction of the two traces (lower panel) reveals the early (arrow) and the late (*) Ca^{2+}-dependent components of the long-lasting after-hyperpolarization.

The most striking aspect of the long-lasting after-hyperpolarization is the slow time to peak of the LAHP. There are two plausible explanations to account for the shape of the long-lasting after-hyperpolarization. (1) Superposition of two conductances for the same ion, with different kinetics; one would reach peak immediately and decay rapidly, while the other would rise slowly, reaching a peak at 1 s and decay slowly. (2) Two conductances with different reversal potentials; one conductance would have a negative reversal potential, a fast rise time and a slow decay, while the second conductance, with a more positive reversal potential, would also have a fast rise time but would be required to decay in roughly 1 s. This second conductance would be responsible for the apparent repolarization and subsequent slowly developing hyperpolarization. The experiments that follow were carried out in order to elucidate the ionic mechanisms that underlie the long-lasting after-hyperpolarization and thereby distinguish between the two alternatives proposed.

Mechanism of generation of the long-lasting after-hyperpolarization

Yarom *et al.* (1985*b*) have established that the long-lasting after-hyperpolarization in these neurones is associated with a fall in the cell input resistance, and that its reversal potential is similar to the reversal potential of the peak of the fast

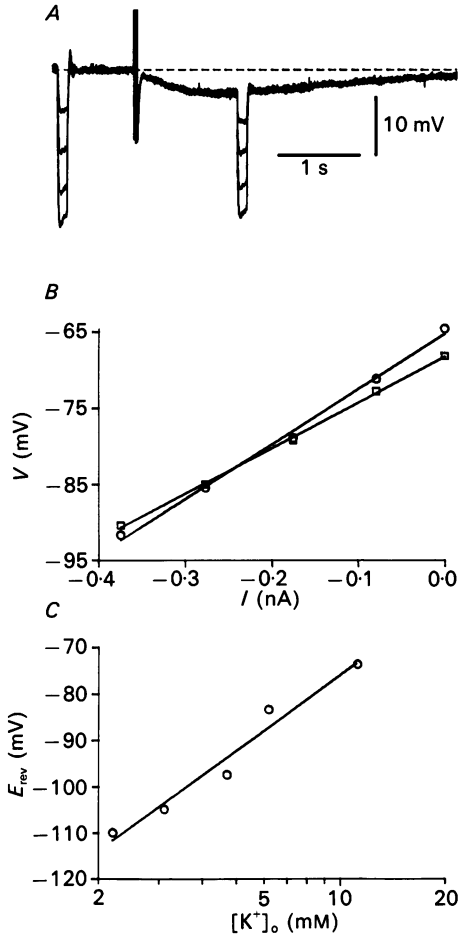

Fig. 4. An increase in potassium conductance underlies the late component of the long-lasting after-hyperpolarization. *A*, four superimposed traces of long-lasting after-hyperpolarizations elicited by trains of three action potentials. The input resistance of the cell at rest and close to the peak of the long-lasting after-hyperpolarization was measured by injections of current pulses of different amplitudes. External K^+ concentration ($[K^+]_o$) was 6·2 mM. *B*, a comparison of the voltage–current relationships at resting level (○) and during the peak of the long-lasting after-hyperpolarization (□) shows a decrease in input resistance (from 72 to 60 MΩ). The reversal potential (intersection between the regression lines) was −84 mV. *C*, the reversal potential, as measured in *B*, increases as a function of $[K^+]_o$. The 54·3 mV per 10-fold change of $[K^+]_o$ suggests that potassium is the most permeant ion during this process.

AHP ($g_{K,H-H}$). In order to determine the ionic conductances underlying the long-lasting after-hyperpolarization, we measured the changes in input resistance of the cell during the peak of the LAHP, calculated its reversal potential and determined its dependence on external K^+ concentration.

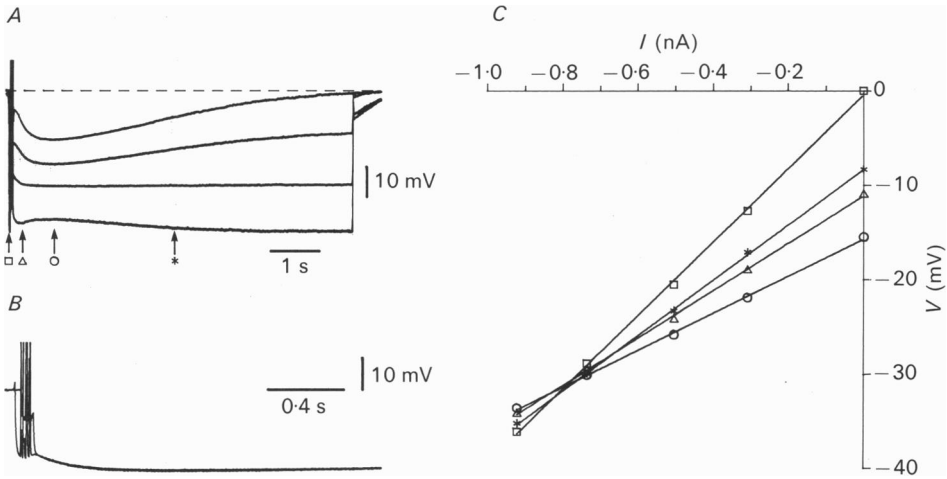

Fig. 5. Continuous measurement of changes in conductance and reversal potential during the long-lasting after-hyperpolarization. *A*, four superimposed traces of long-lasting after-hyperpolarizations elicited by trains of four action potentials. Negative current pulses of different intensities (−0·3, −0·5 and −0·7 nA) were superimposed on the second, third and fourth traces. Current injection started 30 ms before the train of action potentials and lasted 7 s. Note that the long-lasting after-hyperpolarization reversed its polarity at −0·7 nA of current injection. *B*, Current injection prior to and after the train of action potentials does not affect the time course of the long-lasting hyperpolarization. Two superimposed traces of long-lasting after-hyperpolarizations in the presence of −0·5 nA current pulses. In one case, the current injection started 30 ms before the train of action potentials, and 25 ms after the train in the second case. *C*, current–voltage curves measured at the times marked by arrows in *A*. Maximum conductance occurs during the peak of the long-lasting after-hyperpolarization (t = 1000 ms, ○). Note that the three *I–V* relations measured during the long-lasting after-hyperpolarization (△, ○, *) intersect with the resting *I–V* curve (□) at the same point.

The conductance change at the peak of the LAHP was determined by calculating the slope of the *I–V* relation at this point and comparing it to the slope during rest conditions. The experimental method is illustrated in Fig. 4*A*. Negative current pulses (120 ms) of various intensities were delivered before the train of action potentials and close to the peak of the LAHP. The resulting *I–V* relations are shown in Fig. 4*B*. Both curves are reasonably linear. The input resistance at the peak of the LAHP dropped from 72 to 60 MΩ, while the reversal potential, calculated as the intersection between the regression lines, was −84 mV. The experiment was repeated at different concentrations of external potassium, and the calculated reversal potentials were plotted as a function of the external K^+ concentration (Fig. 4*C*). The slope of the best fit is 54·3 mV for a decade change in K^+ concentration, fairly close to the value of 59·8 mV expected at the temperature of 33 °C.

Although we have established that the peak of the LAHP is indeed generated by

the activation of a Ca^{2+}-dependent potassium conductance, the possible involvement of other ions during the initial period of the long-lasting after-hyperpolarization still has to be assessed. For this purpose, a novel procedure to calculate the reversal potential and conductance throughout the long-lasting after-hyperpolarization was developed. The central idea which underlies this procedure is the calculation of the voltage–current relation at different times along the phenomena. The slopes of these curves give the conductance at that time, and the voltage intersections with the *I–V* curve measured at rest give the instantaneous reversal potentials.

The procedure is illustrated in Fig. 5. The long-lasting after-hyperpolarizations in Fig. 5*A* were elicited by four action potentials, superimposed on 7 s negative current pulses of different intensities. As the current intensity increases, the amplitude of the LAHP decreases and at the strongest current, reversed polarity was clearly observed. In order to obtain the resting current–voltage relations, the current pulses started before the train of action potentials. Thus, each train was activated from a different membrane potential level. It is possible, therefore, that different amounts of Ca^{2+} ions will enter the neurone, activating a different intensity of Ca^{2+}-dependent K^+ conductance. However, as shown in Fig. 5*B*, no difference was observed when the hyperpolarizing current pulse began immediately after the train of action potentials, instead of before the train.

The four *I–V* curves shown in Fig. 5*C* were obtained before the spike train (□), during the development of the LAHP ($t = 0{\cdot}7$ s; △), at the peak of LAHP ($t = 1$ s; ○) and at the middle of the decay ($t = 3$ s; *). The curves intersect at the same point, indicating that at each of these three points in time, the increase in conductance, although different, has the same reversal potential. Furthermore, the linearity of the curves, at least in the range of potentials examined, demonstrates that the increase in conductance underlying the long-lasting after-hyperpolarization is not voltage dependent (from resting potential down to 40 mV below rest), thereby strengthening our contention that the amount of Ca^{2+} entering the cell during each action potential is not affected by the membrane potential level.

Figure 6 shows the results of the calculations made at 650 points. The upper trace shows the voltage trajectory at resting potential level following four spikes, the bottom trace gives the calculated changes in conductance and the middle trace the reversal potential. After 300 ms the reversal potential reached a steady-state level, showing that from this time onwards a single process is involved in the generation of the long-lasting after-hyperpolarization. Since we have shown that the peak of the LAHP, which lies within this period, is the result of a Ca^{2+}-activated K^+ conductance (Figs 3 and 4), the entire period after 300 ms can be explained by this process. The conductance time course (lowest trace in Fig. 6), like the time course of the long-lasting after-hyperpolarization itself, reaches a peak only after 1 s, appreciably later than the time when the reversal potential reaches the K^+ equilibrium potential. Thus we conclude that the slow kinetics of the LAHP indeed result from the slow kinetics of channel activation.

Figure 6 also shows that the reversal potential during the first 300 ms is less negative than the potassium equilibrium potential. This finding indicates that an additional conductance participates in the generation of the early part of the long-lasting after-hyperpolarization. Since these conductance changes are rather slow,

capacitative currents can be neglected and the time course of this hypothetical conductance (g_x) can be calculated from the time course of reversal potential changes ($E_{AHP}(t)$) and the conductance changes ($g_{AHP}(t)$).

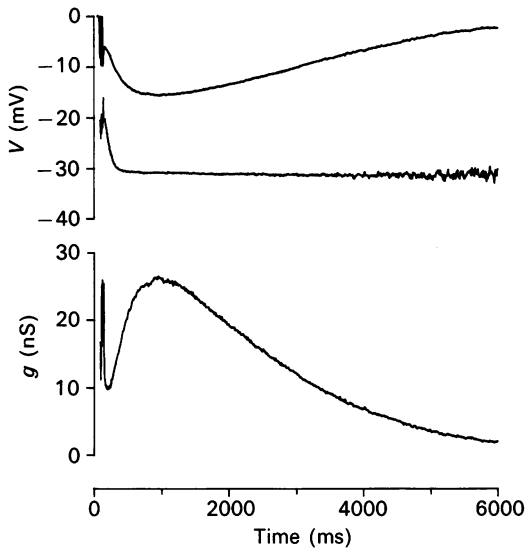

Fig. 6. The time course of the long-lasting after-hyperpolarization reflects the time course of the conductance changes. The changes in conductance and reversal potential calculated from data presented in Fig. 5. Upper trace: time course of long-lasting after-hyperpolarization following a train of four action potentials. Note the characteristic prolonged time to peak (800 ms) of the late component of the long-lasting after-hyperpolarization. Middle trace: time course of the changes in the instantaneous reversal potential. Note that after 300 ms, the reversal potential is constant (31 mV below rest). Lower trace: time course of the increase in conductance during the long-lasting after-hyperpolarization. After a fast initial decrease in conductance, the conductance rises slowly, reaching a peak value at 800 ms.

Since $$E_{AHP}(t) = (g_K(t)\, E_K + g_x(t)\, E_x)/(g_K(t) + g_x(t)),$$

and $$g_{AHP}(t) = g_K(t) + g_x(t),$$

where E_K = the potassium equilibrium potential, E_x = the reversal potential of the hypothetical conductance, and $g_K(t)$ = the time course of the conductance changes of the late component of the long-lasting after-hyperpolarization (LAHP), then

$$g_x(t)\,(E_x - E_K) = g_{AHP}(t)\,(E_{AHP}(t) - E_K).$$

The time course of $g_x(t)$ was calculated for the data presented in Fig. 6, assuming that the K^+ equilibrium potential (E_K) is equal to the steady-state level of $E_{AHP}(t)$ (31 mV below resting) and that (E_x) is equal to the $E_{AHP}(t)$ value at the end of the train of action potentials (11 mV more positive than E_K).

The results of these calculations are shown in Fig. 7. The dotted line represents the first second of the time course of the conductance changes ($g_{AHP}(t)$) from the experiment shown in Fig. 6; the continuous line represents the calculated time course of the hypothetical conductance ($g_x(t)$). The dashed line, which is the difference

between the two, represents the onset of the late component of the after-hyperpolarization. Note that the time course of $g_x(t)$ is independent of the chosen E_x value. If we assume a more positive E_x value, a third conductance with a negative reversal potential and similar time course will have to be postulated to account for the experimentally measured time course of the conductance changes.

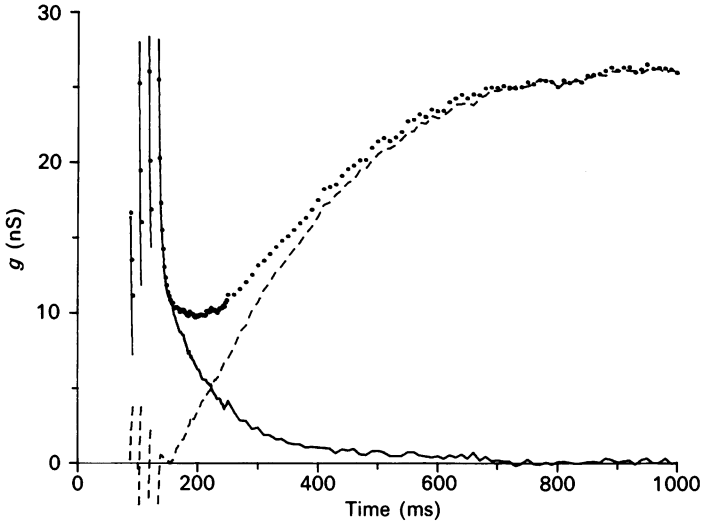

Fig. 7. Calculating the early component of the long-lasting after-hyperpolarization according to the time course of the changes in the reversal potential. Dotted line: the changes in conductance during the long-lasting after-hyperpolarization as calculated from the voltage–current relationship (see Fig. 6). Continuous line: time course of a hypothetical early conductance, $g_x(t)$, as calculated from the changes in reversal potential, assuming that E_x is 20 mV more negative than the resting potential (see text for explanation). Dashed line: the difference between the total change in conductance and the hypothetical *early* conductance; shows the onset of the *late* component of the long-lasting after-hyperpolarization.

These calculations suggest that the long-lasting after-hyperpolarization is composed of two conductances: (1) an early conductance with fast kinetics which reaches its maximum value immediately after the train of the action potentials and decays with a time constant of about 100 ms; (2) a late component with slow kinetics where the conductance reaches a peak in about 1 s and decays over a period of several seconds. This conclusion is in agreement with our previous description of two conductances having different weights participating in the generation of the long-lasting after-hyperpolarization. The additional information, if correct, indicates that the two conductances differ in their reversal potential by about 10 mV.

Differential blockade of the long-lasting after-hyperpolarization by noradrenaline

Fukuda, Taketsugu, Nabekura & Oomura (1987) studied the responses of rat vagal motoneurones to noradrenaline (NA); they reported that these neurones either depolarize in response to NA or hyperpolarize and that these responses were associated with an increase or decrease in neuronal input resistance, respectively. In

our hands, exposure of vagal motoneurones of the guinea-pig to NA usually resulted in depolarization of the cell, associated with an increase in firing rate. The changes in input resistance, however, were less consistent: in seven out of nine cases a decrease of 10% in input resistance occurred, while in the other two cases an increase

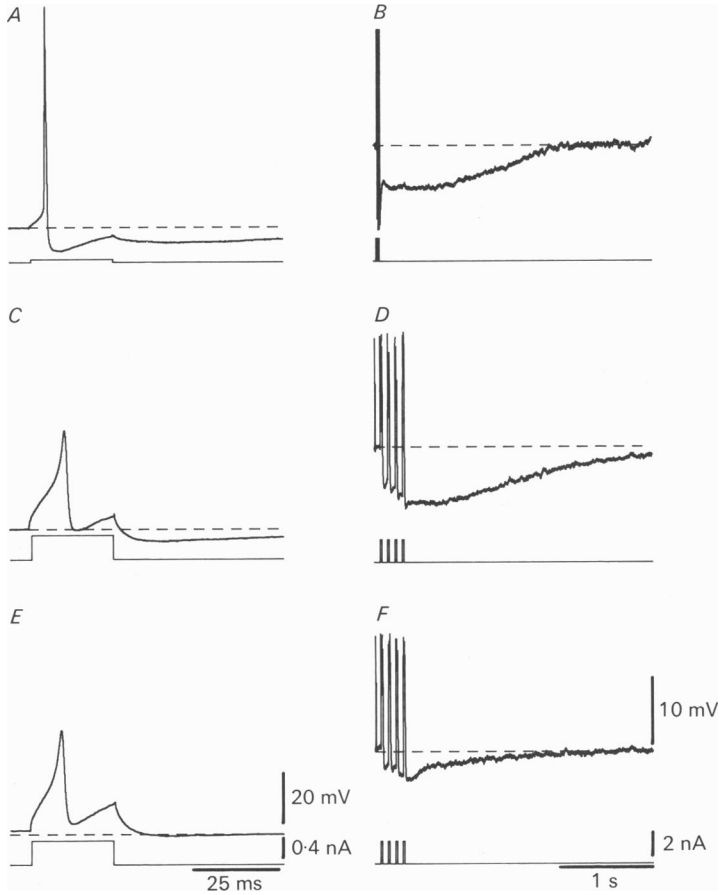

Fig. 8. Noradrenaline blocks the long-lasting after-hyperpolarization without affecting the Ca^{2+}-dependent action potential. *A* and *B*, under control conditions, a current pulse of 0·1 nA (*A*, lower trace) elicits a fast action potential characterized by 95 mV amplitude and 1·2 ms duration. A train of four action potentials generates a long-lasting after-hyperpolarization (*B*). *C* and *D*, in the presence of TTX (10^{-5} M), a stronger current pulse, 0·4 nA (*C*, lower trace) elicits a Ca^{2+}-dependent regenerative response characterized by its low amplitude, long duration and higher threshold. A train of four, TTX-resistant, regenerative responses is followed by a long-lasting after-hyperpolarization (*D*) which behaves similarly to that observed under control conditions. *E* and *F*, in the presence of noradrenaline (NA, 30 μM). The TTX-resistant, regenerative response has not been affected (*E*) although the membrane potential is slightly depolarized (dashed line shows value before addition of NA). The long-lasting after-hyperpolarization, however, is almost completely abolished (*F*).

of 50% in the resistance of the cell was observed. The most conspicuous and reproducible effect, obtained at concentrations as low as 1 μM, was the reduction of the long-lasting after-hyperpolarization without affecting Ca^{2+} influx. Similar

phenomena were described in other preparations (Hass & Konnerth, 1983; Madison & Nicoll, 1984; Yoshimora *et al.* 1987).

An example of this last effect of NA is shown in Fig. 8. Under normal conditions (Fig. 8*A* and *B*), a small current of about 0·1 nA was sufficient to elicit an action

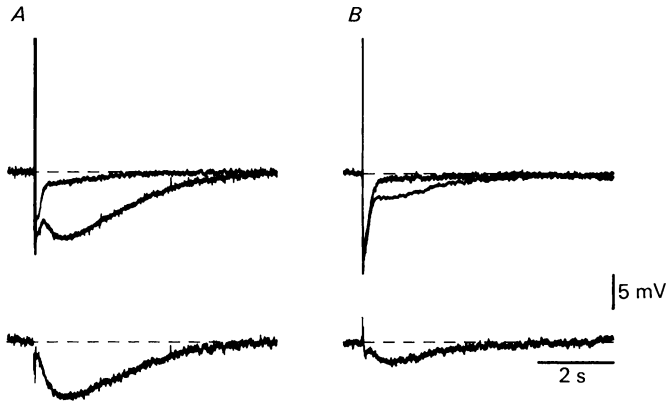

Fig. 9. Noradrenaline blocks the late component of the long-lasting after-hyperpolarization without affecting the early part. *A*, upper panel: two superimposed traces of long-lasting after-hyperpolarizations before and after the addition of NA (50 μM). Note that under control conditions both components of the long-lasting after-hyperpolarization are clearly discernible and that NA specifically affects the late component. Subtraction of the two traces (lower panel) reveals the characteristic time course of the late component of the long-lasting after-hyperpolarization. *B*, the same as in *A* for a different cell where the long-lasting after-hyperpolarization displays a prominent early component. Note that also in this case the subtraction of the two traces reveals the characteristic time course of the late component of the long-lasting after-hyperpolarization.

potential of 95 mV amplitude and 1·2 ms duration. This action potential was followed by an after-hyperpolarization (AHP) that lasted beyond the duration of the current pulse (Fig. 8*A*). A train of four action potentials at 100 Hz (Fig. 8*B*) generated a typical long-lasting after-hyperpolarization. In the presence of 10^{-5} M-tetrodotoxin (TTX), only Ca^{2+}-dependent regenerative responses were observed (Fig. 8*C*). These responses were characterized by a high threshold, low amplitude and longer duration, and were also followed by an after-hyperpolarization. Under these conditions, a train of four action potentials at 10 Hz was followed by a long-lasting after-hyperpolarization similar to that obtained in normal conditions (compare Fig. 8*B* and *D*). Addition of 30 μM-NA in the presence of TTX, although inducing a small depolarization and a reduction of the AHP that followed the action potential, did not affect the threshold, amplitude or duration of the action potential itself (Fig. 8*E*). The long-lasting after-hyperpolarization, on the other hand, was virtually abolished (compare Fig. 8*F* and *D*).

Two examples of the effect of NA on the long-lasting after-hyperpolarization are shown in Fig. 9. The two superimposed traces shown in the upper panel of *A* and *B* represent the responses of two vagal motoneurones to a train of action potentials before and after the application of NA (50 μM). In both examples, a marked reduction in the LAHP is evident, regardless of its relative weight in the long-lasting after-hyperpolarization. Furthermore, subtraction of the two traces (shown in lower

panels of *A* and *B*) shows that the NA-sensitive component has a slow rise time and a long duration, which correspond to features of the time course of the LAHP

In the presence of NA a relatively fast component, similar to the EAHP (see Fig. 1*C*) and resembling the time course of the hypothetical conductance g_x (see Fig. 7)

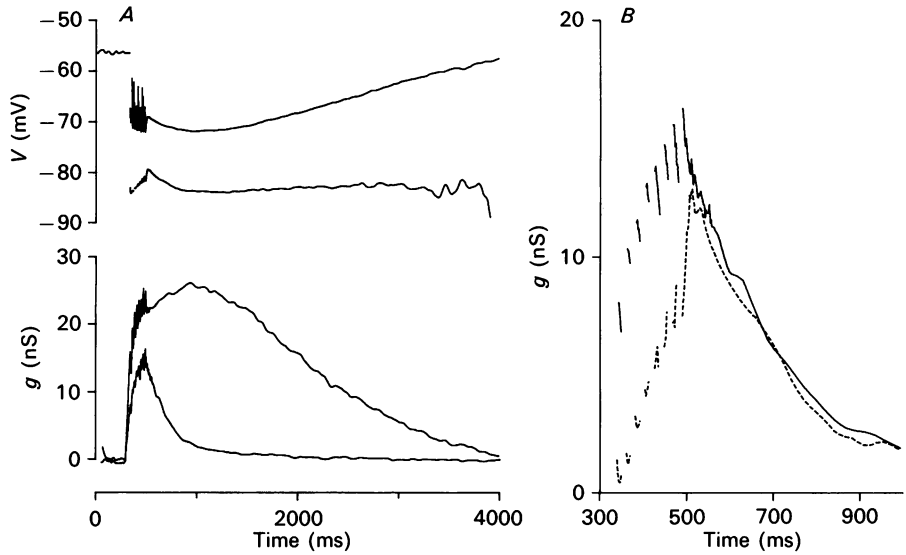

Fig. 10. The time course of the NA-insensitive conductance is similar to the time course of the early component calculated from the changes in reversal potential. *A*, the long-lasting after-hyperpolarization (upper trace) following a train of eight action potentials was used to calculate the reversal potential (second trace) and the change in conductance (third trace) as described in Figs 5 and 6. The lower trace in the conductance panel, was calculated from the after-hyperpolarization elicited by a similar train of action potentials in the same neurone after the addition of NA. *B*, time course of NA-resistant conductance (continuous line) is virtually identical to the calculated time course of the early conductance (g_x, dashed line), assuming a reversal potential value of −75 mV. (This assumption is based on the fact that the reversal potential at the end of the train (−79 mV) is equal to the value of E_x only when short trains of action potentials are used; see text, and Fig. 7.)

was always recorded. The results shown in Fig. 10 demonstrate that the NA-resistant conductance is indeed identical to g_x. The time course of both the conductance changes (Fig. 10*A* third trace) and the reversal potential (Fig. 10*A* second trace) of the after-hyperpolarization, following a train of eight action potentials were calculated as described before. The time course of the conductance changes in the presence of NA was also calculated (Fig. 10*A* lowest trace). The reversal potential was −79 mV at the end of the train and reached a steady-state level of −85 mV after 300 ms. The time course of g_x calculated from the changes in reversal potential, assuming E_x of −75 mV, is shown in Fig. 10*B* (dashed line). Superimposed is the time course of conductance changes observed in the presence of NA (continuous line in Fig. 10*B*). The outstanding similarity strongly suggests that the early part of the long-lasting after-hyperpolarization is generated by a NA-resistant conductance which can be calculated from the time course of the reversal potential changes.

These observations support our previous conclusion that two different calcium-dependent potassium conductances are involved in the generation of the long-lasting after-hyperpolarization. Both components have negative reversal potentials, but the reversal potential of the early component (EAHP) is 10 mV less negative than that of the late component (LAHP). The EAHP reaches its maximum value immediately after the train and decays with a time constant of 100–200 ms. The LAHP slowly develops in about 1 s to a peak value and then decays with a time constant of 2–3 s. Finally, only the LAHP is sensitive to NA in concentrations as low as 1 μM.

Dependence of the LAHP on Ca^{2+} entry

The relationship between the potassium conductance and the internal Ca^{2+} concentration can be evaluated if we assume that a constant amount of Ca^{2+} ions enters the cell during each action potential. This assumption was partly corroborated by optical measurements of light absorption of the Ca^{2+}-sensitive dye Arsenazo III (for methods and procedures see Ross & Werman, 1987). In these preliminary observations it was found that each action potential in a train (up to eleven action potentials) was associated with a constant change in light absorbance. The intracellular Ca^{2+} concentration is, therefore, linearly related to the number of action potentials. The maximum LAHP conductance, on the other hand, can be measured by conventional current clamp techniques. Thus, analysing the relation between the maximum LAHP conductance and the number of action potentials in the train should reveal the nature of the relationship between the Ca^{2+} concentration and the potassium conductance.

In order to measure the peak conductance of the LAHP, a hyperpolarizing current pulse of constant amplitude ($-0{\cdot}1$ nA) and duration (100 ms) was injected before the trains of action potentials and again during the peak of the LAHP. At this time, the contribution of the EAHP to the amplitude of the long-lasting after-hyperpolarization is negligible; therefore, no attempt was made to subtract the EAHP from this measurement. The difference between the membrane responses to the constant current pulse represent the conductance activated by the Ca^{2+} entry. Figure 11*A* shows the behaviour of the LAHP amplitude (□) and the peak change in conductance (●) as a function of the number of action potentials.

The behaviour of the LAHP conductance as a function of the number of spikes is similar to that of the LAHP amplitude. The amplitude, however, seems to saturate at a lower number of action potentials, as expected from the decrease in driving force. The absence of saturation of the conductance changes also suggests that only a small fraction of the Ca^{2+}-dependent potassium channels is activated during the LAHP.

The LAHP conductance seems to rise sigmoidally as a function of the number of action potentials. In order to confirm the apparent sigmoidal relationship, the behaviour of the peak LAHP conductance at low intracellular Ca^{2+} concentrations has to be examined. For that purpose the Ca^{2+} conductance was partially blocked by the addition of 2·0 mM-$CoCl_2$. As a result, the amount of Ca^{2+} entering the cell with each spike was reduced and the LAHP was markedly decreased. The conductance changes obtained in the presence of Co^{2+} ions are shown in Fig. 11*A* (*). When these data were normalized and combined with the data in control conditions (Fig. 11*B*),

they appear to confirm the sigmoidal nature of the relationship between conductance and Ca^{2+} concentration. The method of normalization is based on the observation that the response for four action potentials in the presence of Co^{2+} was similar in amplitude to the response to one action potential in control conditions. Thus, the

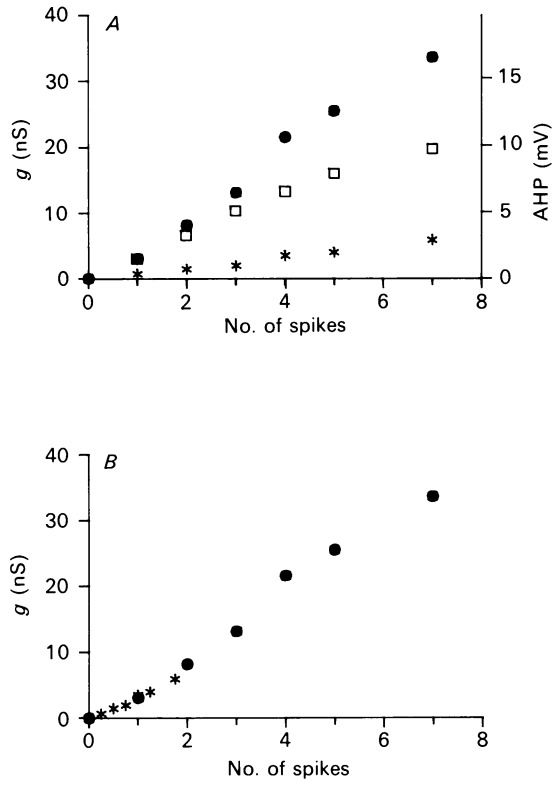

Fig. 11. The maximal conductance of the late component of the long-lasting after-hyperpolarization is a sigmoidal function of the number of action potentials. *A*, maximal amplitude of LAHP (□) and accompanying change in conductance (●) increase as a function of the number of action potentials. Extracellular Ca^{2+} concentration was 2·5 mM. Note that due to a decrease in driving force, the maximal amplitude saturates at a lower number of action potentials than the maximal changes in conductance. *, maximal change in conductance after the addition of 2 mM-Co^{2+} ions to the bath. Note that the values of conductance changes decrease dramatically after addition of cobalt. *B*, the same as in *A* after normalizing the data obtained in the presence of Co^{2+} ions (the number of action potentials was multiplied by 0·25, see text) to form a continuous set of data.

data were normalized by multiplying the number of action potentials in the presence of Co^{2+} by 0·25. The sigmoidal pattern of the peak conductance as a function of the number of action potentials obtained suggests that more than one Ca^{2+} ion is needed to activate the K^+ channel. Since in all ($n = 8$) of our experiments log–log plots of the peak amplitude as a function of the number of action potentials yielded maximal slopes between 1 and 2, we conclude that a minimum of two Ca^{2+} ions are needed to activate a K^+ channel.

Modelling the Ca^{2+}-dependent conductance underlying the LAHP

On the basis of our results, we formulated a model which simulates the slow kinetics of the LAHP. The model is based on the following assumptions:

Ca^{2+} entry. During each action potential a constant amount of Ca^{2+} entered the cell and as a result the intracellular concentration rises by α. Thus, the Ca^{2+} concentration at the end of a train of action potentials can be described as

$$Ca^{2+}_{i,(t=0)} = n\alpha + Ca^{2+}_0,$$

where $Ca^{2+}_{i,(t=0)}$ is the intracellular Ca^{2+} concentration immediately after the train of n action potentials and Ca^{2+}_0 is the resting Ca^{2+} concentration.

The Ca^{2+}-dependent K^+ channels. In accordance with our results we postulate that the binding of two Ca^{2+} ions are needed in order to open a Ca^{2+}-dependent K^+ channel. Therefore, the channel can appear in two closed states and one open state, and the transitions are dependent on the binding of Ca^{2+} ions.

The state model can be formalized as follows:

$$C + Ca^{2+}_i \underset{k_{-1}}{\overset{k_1}{\Leftrightarrow}} C^* + Ca^{2+}_i \underset{k_{-2}}{\overset{k_2}{\Leftrightarrow}} O,$$

where C and C* are dimensionless parameters denoting the probability of the channel being closed, without Ca^{2+} and with one bound Ca^{2+} ion, respectively. O represents the probability of a channel being open.

Ca^{2+} removal. The model assumes that the rate of removal of Ca^{2+} from the cell is proportional to a rate constant β and the difference between the concentration of Ca^{2+} at time t ($Ca^{2+}_{i,t}$) and the resting Ca^{2+} concentration, Ca^{2+}_0:

$$\frac{dCa^{2+}_i}{dt} = -\beta(Ca^{2+}_{i,t} - Ca^{2+}_0).$$

The following equations, which were constructed according to these assumptions, describe the behaviour of the Ca^{2+}-dependent K^+ conductances relative to the postulated time course of the change in intracellular Ca^{2+} concentration:

$$\frac{dC}{dt} = -k_1 Ca^{2+}_i C + k_{-1} C^*, \tag{1}$$

$$\frac{dO}{dt} = -k_2 Ca^{2+}_i C^* - k_{-2} O, \tag{2}$$

$$O + C + C^* = 1, \tag{3}$$

$$Ca^{2+}_{i,t} = Ca^{2+}_0 + n\alpha e^{-\beta t}. \tag{4}$$

The behaviour of the Ca^{2+}-dependent K^+ conductance as predicted by this model is demonstrated in Fig. 12. According to the model the onset of the Ca^{2+}-dependent K^+ conductance is governed by the slow rate constants of the channels, while the decay time is determined by the rate of removal of Ca^{2+} ions. In the absence of the Ca^{2+} removal processes (Fig. 12*A*; $\beta = 0$), the fraction of open channels slowly developed into a steady-state level determined by the rate constants. In order to obtain such a slow opening process, one of the expressions $k_2 Ca^{2+}_i$ or $k_1 Ca^{2+}_i$ as well

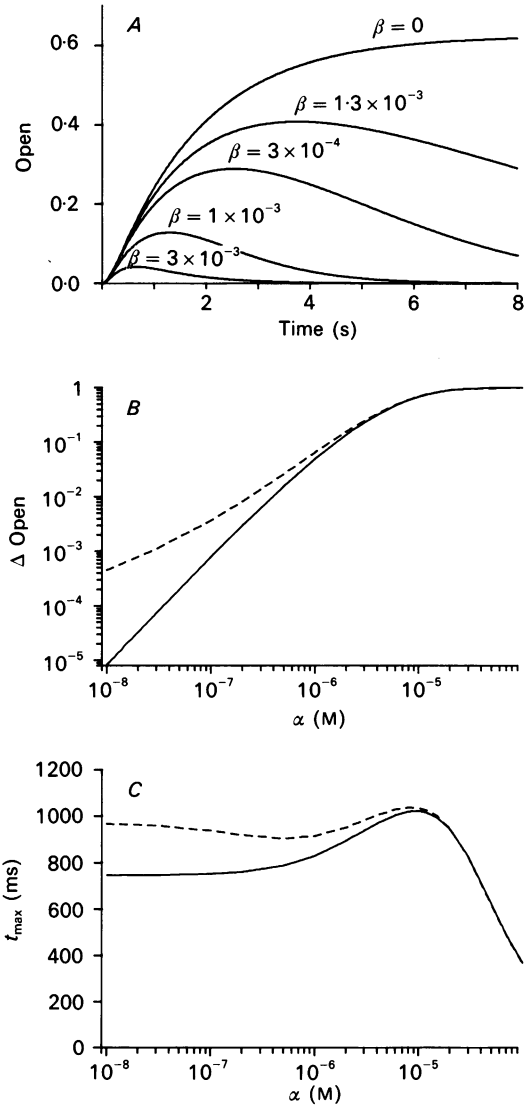

Fig. 12. Predictions of the model: the effect of Ca^{2+} entry, Ca^{2+} removal and resting Ca^{2+} concentration on the time course, amplitude and time to peak of the conductance changes. *A*, increasing the rate of Ca^{2+} removal decreases the amplitude and time to peak of the LAHP conductance. Simulation parameters: $k_1 = 100$ (ms M)$^{-1}$; $k_2 = 10^{+3}$ (ms M)$^{-1}$; $k_{-2} = k_{-1} = 10^{-3}$ ms^{-1}. When internal Ca^{2+} concentration rises from 0 to 5×10^{-6} M and no calcium is removed ($\beta = 0$), the fraction of open channels increases gradually and reaches a steady state. When $\beta > 0$, the fraction of open channels rises to a peak and then decreases. *B*, maximal conductance increases as a function of Ca^{2+} entry (α). Same parameters as in *A*, $\beta = 10^{-3}$ ms^{-1}. In the absence of resting Ca^{2+} (continuous line), the log–log relation has an initial slope of 2. When the resting Ca^{2+} level is higher ($Ca_0^{2+} = 10^{-7}$ M, dashed line), maximal slope is between 1 and 2. *C*, time to peak as a function of Ca^{2+} entry. Same simulations as above. The time to peak shows complex behaviour. It might change from relative stability to points of maxima and/or minima, but it always decreases at high levels of Ca^{2+} entry.

as one of the rate constants, k_{-1} or k_{-2}, had to be sufficiently small. When a removal process is introduced, the fraction of open channels reaches a peak at a time and amplitude determined by the rate of Ca^{2+} removal. As the rate of Ca^{2+} removal (β) increases (Fig. 12*A*, $0 < \beta$), a reduction in peak amplitude and time to peak occurs. It should be noted that if the rate of Ca^{2+} removal (β) is faster than the rate of dissociation of the channel–Ca^{2+} complexes (k_{-1}, k_{-2}), the slower process will determine the decay of the Ca^{2+}-dependent K^+ conductance.

The time to peak and amplitude are strongly affected by the resting Ca^{2+} concentration (Ca_0^{2+}), and the change in Ca^{2+} concentration ($n\alpha$; Fig. 12*B* and *C*). In Fig. 12*B*, the amplitude of the response is expressed on a logarithmic scale as the maximal change in fraction of open channels (Δ Open), while the change in Ca^{2+} concentration, also on logarithmic scale, is expressed in moles per litre. If, at resting conditions $Ca_0^{2+} = 0$ (continuous line), a linear relation with an initial slope of 2 is predicted. However, if resting Ca^{2+} concentration is higher ($Ca_0^{2+} = 10^{-7}$; dashed line) a smaller maximal slope (between 1 and 2) is predicted. Only at high levels of Ca^{2+} concentration change do the two curves merge.

The behaviour of the time to peak as a function of the changes in Ca^{2+} concentrations is shown in Fig. 12*C*. With the rate constants chosen and $Ca_0^{2+} = 0$, an increase in time to peak up to a concentration change of 10^{-5} M is predicted by the model (Fig. 12*C*, continuous line). At higher concentrations, the time to peak should decrease. The presence of a resting Ca^{2+} concentration (10^{-7} M; dashed line) did not change the behaviour of the time to peak at high levels of concentration changes, but strongly affects the behaviour at lower concentration. Instead of an increase in time to peak, a decrease is predicted, which reverses at a concentration change of 10^{-6} M. It should be noted that the time to peak as a function of the changes in Ca^{2+} concentration is critically dependent on the parameters used in the simulation. For example, symmetrical values of the rate constants will result in a monotonic decrease in rise time.

In view of these predictions that show a complex relationship between the time to peak and the change in intracellular Ca^{2+} concentration, we accurately examined the time to peak of LAHPs elicited by trains of action potentials. The time to peak as a function of the number of action potentials was measured in fifteen cells, where the slopes calculated by linear regression were studied. A slope was considered to be significant if the standard deviation value was less than the slope value. A negative slope was found in eight cells, of which only one was non-significant. In all the other cells, which showed a positive slope, only one was significant, three seemed to follow a convex parabolic trajectory, and three had a large scatter of data points that prevented an accurate conclusion. It is likely that these differences in behaviour of the time to peak observed in the physiological experiments reflect the difference in the amount of Ca^{2+} entry as a well as differences in resting Ca^{2+} concentrations. Both parameters are dependent on the size of the cell and density of channels and therefore could vary from cell to cell.

The resemblance of the results of simulations using the model to physiologically observed phenomena and the ability to predict physiological behaviour, although not proof of the validity of the model can be regarded, at least, as supporting the model. For this reason, the ability of the model to predict the time course of the

LAHP conductance elicited by trains of action potentials has been examined. The time course of the NA-sensitive conductance change elicited by a train of five action potentials was calculated. The model parameters that gave the best fit were chosen, the time course of the conductance changes expected for different train sizes were

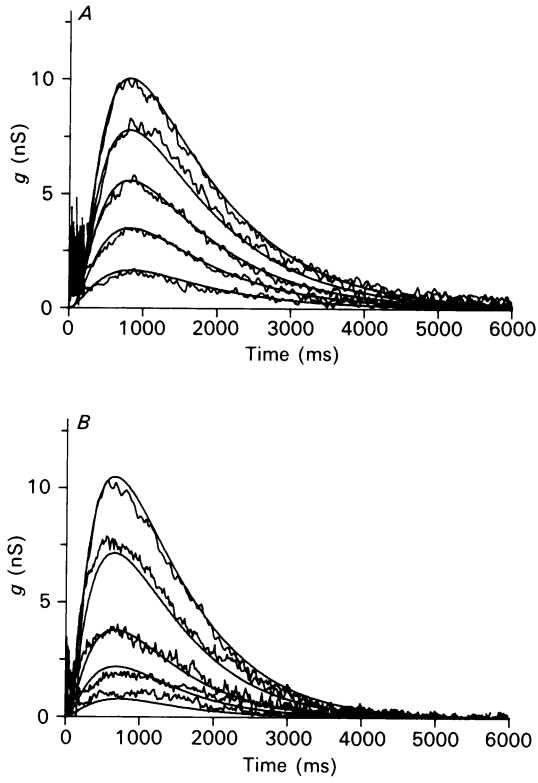

Fig. 13. The time course of the conductance changes predicted by the model match the experimental measurements. *A*, the time course of the conductance changes during LAHPs that followed trains of three, five, seven, nine and eleven action potentials. Temperature, 32·9 °C. Smooth traces are the model predictions with the following parameters: $k_1 = 500$ (ms M)$^{-1}$; $k_{-1} = 2 \times 10^{-3}$ ms^{-1}; $Ca_0^{2+} = 3 \times 10^{-7}$ M; $k_2 = 15$ (ms M)$^{-1}$; $k_{-2} = 3 \times 10^{-3}$ ms^{-1}; $\beta = 0{\cdot}65 \times 10^{-3}$ ms^{-1}; $\alpha = 1{\cdot}4 \times 10^{-6}$ M. *B*, the same as in *A* for a different cell. The LAHPs were elicited by trains of one, two, three, five and seven action potentials. Temperature, 34 °C. The model parameters are the same as in *A* except for $\alpha = 4{\cdot}2 \times 10^{-6}$ M, $\beta = 0{\cdot}9 \times 10^{-3}$ ms^{-1} and $Ca_0^{2+} = 3 \times 10^{-7}$ M. Note that in both cases the model quite accurately predicts the behaviour of the conductance changes. Note also that in both cases the same rate constants, k_j, were used.

then calculated using these parameters, and the simulations compared to the experimental results. During the latter process, re-adjustment of the parameters was occasionally needed. The end result was a set of parameters which predicted quite well the behaviour of the LAHP conductance elicited by trains composed of different numbers of action potentials.

The results are shown in Fig. 13*A*. The time course of the LAHP elicited by trains of three, five, seven, nine and eleven action potentials are shown. The smooth lines

are the predicted time courses; these can be seen to fit the experimental results almost perfectly. The following parameters were used: $k_1 = 500$ (ms M)$^{-1}$; $k_{-1} = 2 \times 10^{-3}$ ms^{-1}; $Ca_0^{2+} = 3 \times 10^{-7}$ M; $k_2 = 15$ (ms M)$^{-1}$; $k_{-2} = 3 \times 10^{-3}$ ms^{-1}; $\beta = 0{\cdot}65 \times 10^{-3}$ ms^{-1}; $\alpha = 1{\cdot}4 \times 10^{-6}$ M. If the model properly describes the processes which associate Ca^{2+} entry with the activation of the Ca^{2+}-dependent potassium conductance, it is expected that the rate constants of these processes will be the same in different cells. On the other hand parameters like channel or ionic pump densities and surface-to-volume ratio, which determine the amount of Ca^{2+} influx, Ca^{2+} removal and resting Ca^{2+} concentration, might differ in different cells. Therefore, the parameters k_1, k_{-1}, k_2, k_{-2}, should have the same values while β and α might vary in different cells. The example shown in Fig. 13*B* supports this possibility. In this example, compared to that of Fig. 13*A*, in addition to the higher amplitude (namely, shorter trains elicit similar responses), a faster development (a shorter time to peak and faster decay) of the LAHP conductance was observed. The predictions of the model, which almost perfectly match the experimental results, were calculated with the following parameters: $Ca_0^{2+} = 3 \times 10^{-7}$ M; $\beta = 0{\cdot}9 \times 10^{-3}$ ms^{-1}; $\alpha = 4{\cdot}2 \times 10^{-6}$ M. The rate constants k_1, k_{-1}, k_2, k_{-2} were the same as those in Fig. 13*A*. It is concluded, therefore, that this simple model is sufficient to account for most of the physiologically observed phenomena.

It should be emphasized that, although the model gives us a great measure of freedom of choice of parameters, there are some constraints on the parameters. The lowest value of the dissociation rate constants, k_{-1} and k_{-2}, or twice the rate of removal of free Ca^{2+}, 2β, gives the final decay rate of the conductance underlying the LAHP, a rate that can be measured experimentally. The time to peak and the behaviour of the time to peak as a function of number of spikes provides more information about either the dissociation constants or the rate of removal, while the behaviour of the amplitude with the number of action potentials gives approximate values for the ratio between association and dissociation constants.

DISCUSSION

In this study, standard current clamp experiments were combined with an original procedure to analyse the mechanism of generation of the long-lasting after-hyperpolarization and characterize the kinetics of the underlying conductances. On the basis of this analysis we concluded that in vagal motoneurones two conductances – which differ in their kinetic properties, selectivity and pharmacological sensitivity – participate in the generation of the long-lasting after-hyperpolarization. The variety of shapes and amplitudes of the after-potentials found in different vagal neurones can be attributed to differences in the relative contribution of each of these conductances to the long-lasting after-hyperpolarization.

The early component (EAHP)

The early component of the long-lasting after-hyperpolarization (EAHP) is a fast developing, Ca^{2+}-dependent conductance that is elicited by the entry of Ca^{2+} during a train of action potentials. The accurate time course of this conductance could be

either measured experimentally, after blocking the late component with NA, or calculated from the changes in reversal potential. The decay time constant of this conductance is in the range of 100–200 ms, and its reversal potential is about 10 mV less negative than that of the late component. The difference in reversal potential is either due to differences in selectivity of the two conductances or to differences in the spatial distribution of the channels. Even if both conductances had the same reversal potential but the EAHP conductance was predominantly located proximally to the conductance of the LAHP, a more negative reversal potential of the LAHP would be expected. Measurements of passive electrotonic spread of potentials in vagal motoneurones (Nitzan, Segev & Yarom, 1990), however, show that their passive properties cannot account for a 10 mV difference in reversal potential (20 mV below rest for EAHP and 30 mV below rest for LAHP). An average voltage attenuation factor of 1·24 was calculated while 1·5 is needed to explain the observed differences. Thus we conclude that the differences in reversal potential reflect a real difference in selectivity of the channels.

The presence of Ca^{2+}-dependent K^+ conductances with kinetic properties similar to the EAHP conductance has been reported in other mammalian neurones (Fowler, Greene & Weinreich, 1985; Lancaster & Adams, 1986; Yoshimura *et al.* 1986; Lancaster & Nicoll, 1987; Ritchie, 1987; Storm, 1989; Williamson & Alger, 1990). In some reports it has been shown that the reversal potentials of these conductances were less negative than that of the LAHP conductance (Brown & Griffith, 1983; Fowler *et al.* 1985; Alger & Williamson, 1988; Storm, 1989). Thus, although we have not ruled out the possibility that the early conductance is a Ca^{2+}-dependent chloride conductance (we did confirm the insensitivity of the EAHP to Cl^- ions in the recording electrode, not shown), the similarity of this conductance to other Ca^{2+}-dependent K^+ conductances (see above) appears to justify the conclusion that the early component is indeed at least partially a Ca^{2+}-dependent K^+ conductance. On the other hand, it seems unlikely that the early component of the AHP, like the 'medium duration AHP' of other neurones (Storm, 1989; Williamson & Alger, 1990) is generated by M-like or Q-like currents. This conclusion is based on the fact that vagal neurones do not respond to cholinergic drugs (Yarom, Bracha & Werman, 1985*a*) nor do they show any anomalous rectification (Nitzan *et al.* 1990).

The late component (LAHP)

The characteristic features of the late component can be summarized as follows. It is a highly selective potassium conductance, which increases with intracellular Ca^{2+} concentration, showing an apparent co-operativity of 2. It is blocked by NA at concentrations as low as 1 μM and it does not show any voltage dependence in the hyperpolarizing potential range. This conductance develops slowly, reaching its peak in 1 s at 33 °C, while decaying over a period of 5–8 s. The presence of a slowly developing Ca^{2+}-dependent K^+ conductance with similar characteristics to that of the vagal motoneurones has been reported using both current clamp methods (Gustafsson & Wigstrom, 1981; Morita, North & Tomikasa, 1982; Fowler *et al.* 1985; Lancaster & Nicoll, 1987) and voltage clamp techniques (Lancaster & Adams, 1986; Storm, 1989). In our work the possibility that the slow development of the late component results from masking by a depolarizing conductance has been ruled out

by concomitantly measuring the changes in reversal potential with the conductance, thus confirming the slow kinetics of the underlying conductance.

The relationship between the transient change in intracellular Ca^{2+} concentration and the kinetics of the Ca^{2+}-dependent conductances

In several studies that characterize the properties of Ca^{2+}-dependent conductances, it has been assumed that the slow time course of these conductances follows the time course of a transient change in Ca^{2+} concentration (Barish & Thompson, 1983; Kuba *et al.* 1983). Such an assumption cannot be reconciled with the presence of two different Ca^{2+}-dependent conductances showing very distinct kinetic properties.

One possible way to explain the different kinetics of these conductances is to assume that the early conductance is voltage dependent in addition to its Ca^{2+} dependence. Such voltage dependence has been demonstrated in several neuronal types (Adams, Constanti, Brown & Clark, 1982; Brown & Griffith, 1983; Lancaster & Nicoll, 1987; Lancaster & Pennefather, 1987; Storm, 1987) and implies, that the K^+ channels may open as a result of fast, voltage-dependent binding of Ca^{2+} to the channels, while the decay time may reflect a decrease in the affinity of the channels for Ca^{2+} during repolarization, rather than a decay in Ca^{2+} concentration (Lancaster, Nicoll & Perkel, 1991).

Another possible explanation to account for the different kinetics of the two conductances is to assume that they are located at different sites along the soma dendritic membrane (Lancaster & Nicoll, 1987). If calcium enters the cell at the soma and then diffuses throughout the cell into the dendrites, and if the early conductance is located at the soma level while the late component is located at the far end of the dendrites, then the different kinetics would reflect different time courses of change in Ca^{2+} concentration at the two sites. It should be emphasized, however, that the different sensitivity to noradrenaline strongly indicates that there are two different channels. Thus, while such an explanation can account for the different kinetics it does not eliminate the need to postulate two different K^+ conductances.

Finally, it is possible that the basic assumption that Ca^{2+} concentration reaches its maximum level at the end of the train is incorrect and, in fact, Ca^{2+} concentration peaks at a later time due to the release of Ca^{2+} ions from intracellular stores (Kuba *et al.* 1983; Constanti & Sim, 1987; Berridge & Irvine, 1989). In this case the slow kinetics would describe the process of Ca^{2+} release rather than the opening of the channels. It should be mentioned that the hypothetical release of Ca^{2+} ions from intracellular stores cannot be triggered by Ca^{2+} ions. A Ca^{2+}-dependent release of Ca^{2+} implies positive feedback and therefore it is hard to reconcile it with the graded response to a rising number of action potentials, unless an additional very powerful negative feedback is also postulated.

Modelling the kinetics of the late component

In this work we have examined the possibility that the slow kinetics of the LAHP conductance reflects very slow rate constants of the channels themselves. For that purpose we constructed a model that is based on the following assumptions: (1) a train of action potentials elicits a Ca^{2+} concentration change that decays

exponentially immediately after the train; (2) each action potential contributes the same amount of Ca^{2+} ions; and (3) Ca^{2+} ions interact with the channel with a co-operativity of 2. This model quite accurately simulates the time course of the late component and predicts the changes that occur as a result of increasing the number of action potentials. In addition, the model provides an explanation for the observed variation in the behaviour of the LAHP time to peak as a function of the number of action potentials.

Although the predictions of the model closely resemble the experimental data, this is not a proof of its validity. There may be more steps before the opening of the channel than postulated by the model or, the very slow rate constants needed to simulate the kinetics of the conductance increase may reflect the mediation of a slow enzymatic process before the actual opening of channels takes place. A study of the kinetics of this conductance increase at the level of single channels may help to clarify the mechanisms underlying its slow development.

This work was supported by a grant from Yad Ha-Nadiv.

REFERENCES

ADAMS, P. R., CONSTANTI, A., BROWN, D. A. & CLARK, R. B. (1982). Intracellular Ca^{2+} activates a fast voltage-sensitive K^+ current in vertebrate sympathetic neurones. *Nature* **296**, 746–749.

ALGER, B. E. & WILLIAMSON, A. (1988). A transient calcium-dependent potassium component of the epileptiform burst after-hyperpolarization in the rat hippocampus. *Journal of Physiology* **399**, 191–205.

BARISH, M. E. & THOMPSON, S. H. (1983). Calcium buffering and slow recovery kinetics of calcium-dependent outward current in molluscan neurones. *Journal of Physiology* **337**, 201–219.

BERRIDGE, M. J. & IRVINE, R. F. (1989). Inositol phosphates and cell signalling. *Nature* **341**, 197–204.

BROWN, D. A. & GRIFFITH, W. H. (1983). Calcium-activated outward current in the voltage-clamped hippocampal neurones of the guinea-pig. *Journal of Physiology* **337**, 287–301.

CONSTANTI, A. & SIM, J. A. (1987). Calcium-dependent potassium conductance in guinea-pig olfactory cortex neurones *in vitro*. *Journal of Physiology* **387**, 173–194.

FOWLER, J. C., GREENE, R. & WEINREICH, D. (1985). Two calcium-sensitive spike after-hyperpolarizations in visceral sensory neurones of the rabbit. *Journal of Physiology* **365**, 59–75.

FUKUDA, A., TAKETSUGU, T., NABEKURA, J. & OOMURA, Y. (1987). The effects of noradrenaline on neurones in the rat dorsal motor nucleus of the vagus, *in vitro*. *Journal of Physiology* **393**, 213–231.

GUSTAFSSON, B. & WIGSTROM, H. (1981). Evidence for 2 types of afterhyperpolarization in CA1 pyramidal cells in the hippocampus. *Brain Research* **206**, 462–468.

HASS, H. L. & KONNERTH, A. (1983). Histamine and noradrenaline decrease calcium-activated potassium conductance in hippocampal pyramidal cells. *Nature* **302**, 432–434.

HERMAN, A. & GORMAN, A. L. F. (1981). Effects of 4-aminopyridine on potassium currents in a molluscan neuron. *Journal of General Physiology* **78**, 63–86.

HOCHERMAN, S., WERMAN, R. & YAROM, Y. (1988). Discerning multiple conductances using a novel method to analyze voltage records. *Society for Neuroscience Abstracts* **14**, 143.

KUBA, K., MORITA, K. & NOHMI, N. (1983). Origin of calcium ions involved in the generation of a slow afterhyperpolarization in bullfrog sympathetic neurones. *Pflügers Archiv* **399**, 194–202.

LANCASTER, B. & ADAMS, P. R. (1986). Calcium-dependent current generating the afterhyperpolarization of hippocampal neurons. *Journal of Neurophysiology* **55**, 1268–1282.

LANCASTER, B. & NICOLL, R. A. (1987). Properties of two calcium-activated hyperpolarizations in rat hippocampal neurones. *Journal of Physiology* **389**, 187–203.

LANCASTER, B., NICOLL, R. A. & PERKEL, D. J. (1991). Calcium activates two types of potassium channels in rat hippocampal neurons in culture. *Journal of Neuroscience* **11**, 23–30.

LANCASTER, B. & PENNEFATHER, P. (1987). Potassium currents evoked by brief depolarizations in bull-frog sympathetic ganglion cells. *Journal of Physiology* **387**, 519–548.

LLINAS, R. & SUGIMORI, M. (1980). Electrophysiological properties of *in vitro* Purkinje cell dendrites in mammalian cerebellar slices. *Journal of Physiology* **305**, 171–195.

MADISON, D. V. & NICOLL, R. A. (1984). Control of the repetitive discharge of rat CA1 pyramidal neurones *in vitro*. *Journal of Physiology* **372**, 245–259.

MARTY, A. (1989). The physiological role of the calcium-dependent channels. *Trends in Neurosciences* **12**, 420–424.

MEECH, R. W. & STANDEN, N. B. (1975). Potassium activation in *Helix aspersa* neurones under voltage clamp: a component mediated by calcium influx. *Journal of Physiology* **249**, 211–239.

MORITA, K., NORTH, R. . & TOMIKASA, T. (1982). The calcium-activated potassium conductance in guinea-pig myenteric neurones. *Journal of Physiology* **329**, 341–354.

NITZAN, R., SEGEV, I. & YAROM, Y. (1990). Voltage behavior along the irregular dendritic structure of morphologically and physiologically characterized vagal motoneurons in the guinea pig. *Journal of Neurophysiology* **63**, 333–346.

RITCHIE, A. K. (1987). Two distinct calcium-activated potassium currents in a rat anterior pituitary cell line. *Journal of Physiology* **385**, 591–609.

ROSS, W. N. & WERMAN, R. (1987). Mapping calcium transients in the dendrites of Purkinje cells from the guinea-pig cerebellum *in vitro*. *Journal of Physiology* **389**, 319–336.

STORM, J. F. (1987). Action potential repolarization and a fast after-hyperpolarization in rat hippocampal pyramidal cells. *Journal of Physiology* **385**, 733–759.

STORM, J. F. (1989). An after-hyperpolarization of medium duration in rat hippocampal pyramidal cells. *Journal of Physiology* **409**, 171–190.

WILLIAMSON, A. & ALGER, B. E. (1990). Characterization of an early afterhyperpolarization after a brief train of action potentials in rat hippocampus neurons in vitro. *Journal of Neurophysiology* **63**, 72–81.

YAROM, Y., BRACHA, O. & WERMAN, R. (1985*a*). Intracellular injection of acetylcholine blocks various potassium conductances in vagal motoneurons. *Neuroscience* **16**, 739–752.

YAROM, Y., SUGIMORI, M. & LLINAS, R. (1985*b*). Ionic currents and firing patterns of mammalian vagal motoneurons *in vitro*. *Neuroscience* **16**, 719–737.

YOSHIMURA, M., POLOSA, C. & NISHI, S. (1986). Afterhyperpolarization mechanism in cat sympathetic preganglionic neuron *in vitro*. *Journal of Neurophysiology* **55**, 1234–1246.

YOSHIMURA, M., POLOSA, C. & NISHI, S. (1987). Noradrenaline-induced after-depolarization in cat sympathetic preganglionic neurons *in vitro*. *Journal of Neurophysiology* **57**, 1314–1337.